International Journal of Medical, Medicine and Health Sciences
ISSN: 2517-9969
Vol:8, No:9, 2014

A Virtual Electrode through Summation of Time Offset Pulses

Isaac Cassar, Trevor Davis, Yi-Kai Lo, Wentai Liu

***Abstract*—**Retinal prostheses have been successful in eliciting visual responses in implanted subjects. As these prostheses progress, one of their major limitations is the need for increased resolution. As an alternative to increasing the number of electrodes, virtual electrodes may be used to increase the effective resolution of current electrode arrays. This paper presents a virtual electrode technique based upon time-offsets between stimuli. Two adjacent electrodes are stimulated with identical pulses with too short of pulse widths to activate a neuron, but one has a time offset of one pulse width. A virtual electrode of twice the pulse width was then shown to appear in the center, with a total width capable of activating a neuron. This can be used in retinal implants by stimulating electrodes with pulse widths short enough to not elicit responses in neurons, but with their combined pulse width adequate to activate a neuron in between them.

***Keywords*—**Electrical stimulation, Neuroprosthesis, Retinal implant, Retinal Prosthesis, Virtual electrode.

I. Introduction

RETINAL prostheses seek to restore vision to those who experience partial or total blindness due to retinitis pigmentosa (RP) and age-related macular degeneration (AMD). Although the diseases destroy the photoreceptors in the eyes and significantly alter the composition of the retina, they seem to leave behind a remnant of functional retinal ganglion cells (RGCs) that are able to transmit visual signals to the brain [1], [2]. Epi-retinal prostheses rely upon an array of electrodes that are implanted onto the retina in order to electrically stimulate these functional RGCs. Results have been promising thus far, with successes in eliciting visual responses in subjects that can be used to detect brightness, read large letters, and detect directional movement [3], [4].

Unfortunately, one of the great challenges of these prostheses is the selectivity of individual RGCs. Functional vision would require the ability to systematically stimulate small groups of neurons near an electrode. The Argus II, currently the only FDA approved retinal prosthesis, has 60 electrodes, each 200 μm in diameter [5]. Considering that the human eye contains 1.2-1.5 million RGCs, it becomes clear that these 60 electrodes are inadequate on their own in effectively stimulating specific, localized neurons [6]. Another useful comparison is to television: High Definition is usually defined as 1920x1080 pixels; that is over 2 million total pixels. Compare that to the 60 effective 'pixels' obtainable from the Argus II and the problem becomes apparent.

The obvious solution is to create higher density electrode arrays to increase the resultant image resolution, and these are in development. However, with increased electrode density comes with a variety of problems. High density dictates that the electrodes should be small, but small electrodes run the risk of having a high charge density that can kill adjacent neurons [7]. In addition, there are a number of technological obstacles to overcome such as data transfer, wireless power, and stimulator design that must be accounted for [8]. Instead of simply adding additional electrodes to increase resolution, we propose to use stimulation parameters to create a unique type of virtual electrode located between two existing electrodes.

Virtual electrodes have been shown to appear between adjacent electrodes when they are both stimulated concurrently and have been able to elicit some neural responses in cochlear implants [9], [10]. However, these require a potential peak between the two electrodes, which may or may not occur depending on the spacing of the two electrodes and the amount of current injected. It also includes the risk of additionally stimulating neurons directly above the two stimulating electrodes, which is non-ideal. In our case, we have created a virtual electrode through a similar, yet fundamentally different approach. The theory behind our virtual electrode is based upon the dependency of pulse width on RGC activation. It has been shown that at sufficiently short pulse widths retinal degenerated mice RGCs will not respond to external stimulation [11]. Using this knowledge, the idea is to stimulate two adjacent electrodes with a short enough pulse width that they each fail to stimulate neurons directly above them. However, through constructive interference a virtual electrode of twice the pulse width should appear at the center point between the two electrodes. This virtual electrode should always appear, independent of electrode spacing, and should prevent undesired RGC activation directly above the stimulating electrodes.

II. Materials and Methods

A. Recording Device

In order to mimic the operation of a real retinal implant, we designed a three-axis voltage probe that is able to quantitatively record the potential/electric field above a stimulating electrode array (Fig. 1). The probe was used to obtain various scans above the electrode surfaces from which the pulse width, potential, and activating function of the physical and virtual electrodes could be determined.

Isaac Cassar and Trevor Davis are undergraduate bioengineers at UCLA, Los Angeles, CA 90095 USA (phone: 831-319-8483; e-mail: icazzar@gmail.com, sdtrevordavis@gmail.com).

Yi-Kai Lo and Wentai Liu are with the University of California, Los Angeles, CA 90095, USA (e-mail: yikai.lo@ucla.edu, wentai@ucla.edu).

The project is partially supported by grants from California Capital Equity LLC, UC Laboratory Research Fee Program, and NSF ERC BMES.

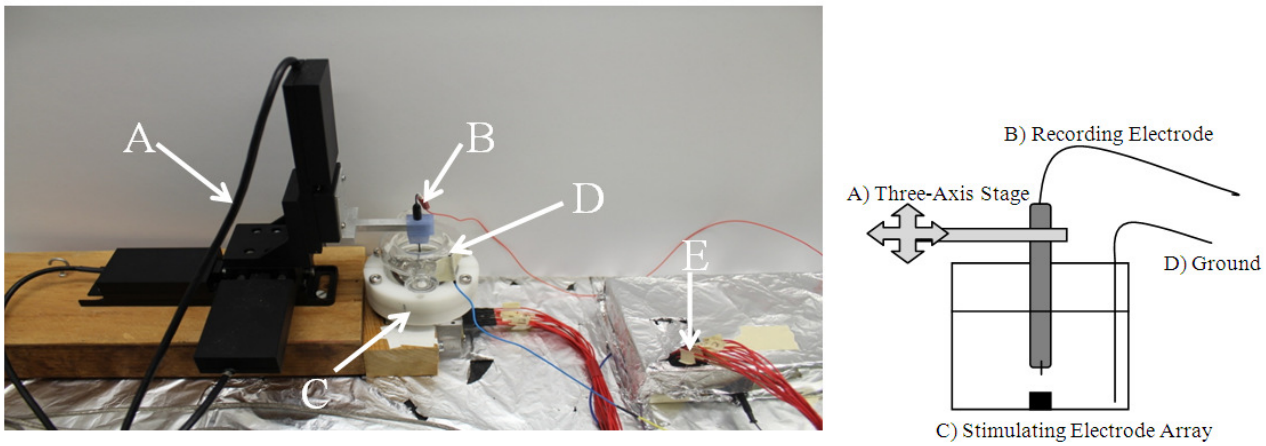

Fig. 1 Schematic of experimental set up. Our system is composed of: [A] a three-axis motor stage, [B] a recording electrode, [C] a microelectrode array placed in a glass with saline, [D] a ground, and [E] an ASIC stimulator

The probe used is a 10 µm diameter platinum microelectrode (BASI, model: MF-2005), which is securely mounted to an arm on a three-axis stage with a spatial resolution of 5 µm. A custom LabView program was made to control the stage motors and process the potential data recorded from the probe via a data acquisition card (National Instruments, model: NI USB-6259). The program has a graphical user interface (GUI) that allows for automatic 3D scanning above a designated region of the electrode array (Fig. 2). It also offers a variety of recording modes such as recording the peak-to-peak voltage, peak cathodic voltage, peak anodic voltage, or the entire waveform at each location. In addition, it offers a variety of filters and graphical displays for the output waveform. In the experiment conducted in this paper, the probe scanned horizontally along a cross-section of the electrodes at a height of 100 µm. It recorded data every 5µm-10µm, depending on the scan.

B. Electrode Array

A 4x4 electrode array composed of 200 µm diameter platinum electrodes with a pitch of 500 µm is used in the experiment. Constant current stimulus provided by our custom retinal application specific integrated circuit (ASIC) stimulator with independent channel stimulation is adopted to produce biphasic stimulus with precise amplitude control and temporal offsets among channels [12]. The electrodes were placed in the center of a cylindrical tank with a diameter of 29 mm and a height of 45 mm (see Fig. 1). A ground electrode was placed along the edge of the tank. The electrodes were immersed in 0.9% w/v saline solution.

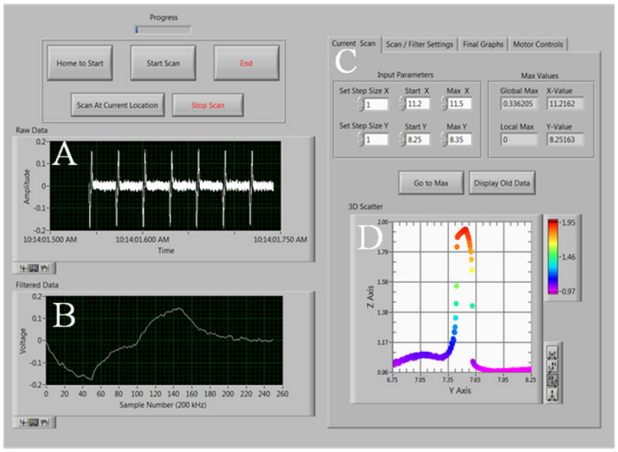

Fig. 2 GUI interface for LabView program. [A] Raw output waveform, [B] Filtered waveform for single pulse, [C] Scan settings, [D] Cumulative 3D graph displaying recorded values for each scanned position

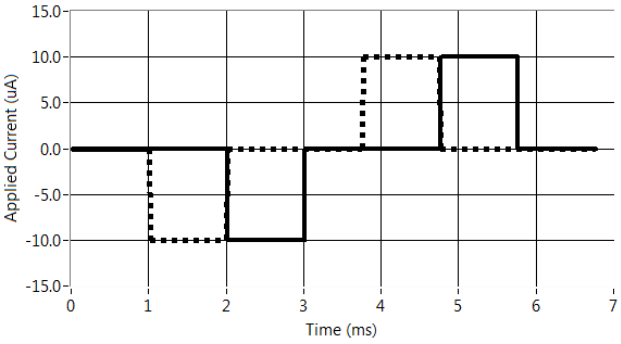

Fig. 3 Combined applied stimulus for adjacent electrodes. The dashed and solid lines represent the individual applied currents to each respective electrode. Both electrodes have the same stimulation parameters except the solid line has a 1 ms time delay. When combined they form a waveform with a 2 ms pulse width

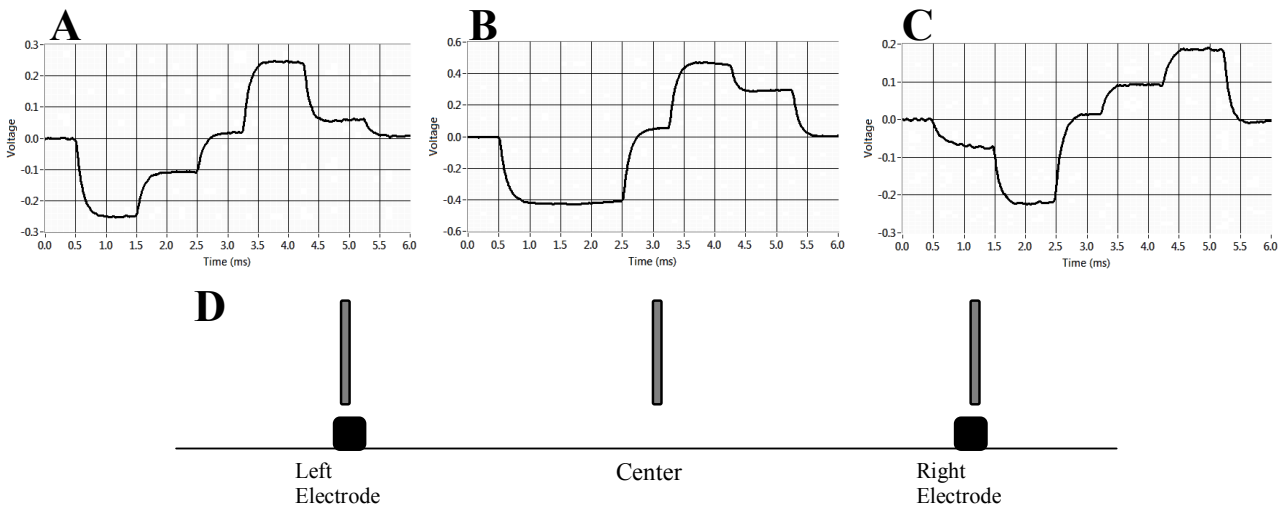

Fig. 4 Recorded voltage waveforms as probe moves along electrodes. [A], [B], and [C] are the waveforms with voltage on the y axis and time in ms on the x axis, with their locations corresponding to the probe positions in [D]. [A] is positioned above the left electrode, [B] is positioned above the center point, and [C] is positioned above the right electrode

C. Stimulation Parameters

We accomplished our virtual electrode stimulating parameters through stimulating one electrode with a 10 μA biphasic current, cathode first, with 1 ms pulse width and a 1.75 ms interphase delay. The other electrode was stimulated with the same parameters except with a 1 ms start delay. 10 μA was chosen because it is still within the range of threshold currents, yet it is smaller than that used for the traditional virtual electrode approach [9], [13]. Large currents create heat that can damage the eye, so we desired to see if our virtual electrode could be created using small currents that are safer for both the eye and the electrodes. Reiterating the theory behind our virtual electrode, it has been shown in [11] that a short pulse width of 40 μs is unable to activate a neuron, whereas an 80 μs pulse width will. A stimulus pulse width of 40 μs would thus be desired for actual stimulation of neurons. As a proof-of-concept, in this experiment, we use a 1 ms stimulus pulse width that allows us to obtain reliable measurements from the DAQ card directly and to validate the virtual electrode theory. We envision that the pulse width can be further scaled down while the virtual electrode can still be created since saline or vitreous humor is simply passive conductive medium.

Fig. 3 shows the waveform of the two applied stimuli and how they should theoretically combine to form a single biphasic pulse with a 2 ms pulse width and a 0.75 ms interphase delay.

III. Results

In order to quantitatively determine whether a virtual electrode with a pulse width of 2 ms appeared between the two electrodes, we used our recording device to scan along a linear cross-section of the two electrodes. Both electrodes were stimulated with the previously described stimulation parameters. The electrode designated as 'left' has the stimulation with no start delay and the electrode designated as 'right' has the 1 ms start delay. First, a scan was done to record the potential waveform at each point along the electrodes. From this scan we can see how the two waveforms interact (Fig. 4). Above each electrode its own respective signal dominates: above the left electrode the cathodic voltage peaks from 0.5 – 1.5 ms and above the right electrode the cathodic voltage peaks from 1.5 – 2.5 ms. However, in the center they both contribute equally, forming a steady peak from 0.5 – 2.5 ms.

A second scan was done which recorded the peak cathodic voltage at each point along the electrode array (Fig. 5). This helps us to understand how the magnitude of the potential changes with position. From Fig. 5 we can also easily determine the locations for both of the stimulating electrodes based off of the negative peaks: by defining the middle point between the two peaks as 0.0 mm, both electrodes are located approximately 250 μm on either side of the center. This is supported by the fact that it is known that the electrodes in the array are separated by 500 μm from center-to-center. The left electrode has a slightly lower (less negative) peak than the right electrode, but this is most likely due to slight surface differences between the two electrodes and should have a minimal effect on the results and the virtual electrode effect.

A third scan was done along the same cross-section which recorded the pulse width at each point (Fig. 6). The pulse width was recorded through the pre-existing Pulse Measurements signal analysis function within LabView. From Fig. 6 it can be seen that the pulse width is approximately 1 ms everywhere except -0.1 mm – 0.1 mm, where it peaks at approximately 1.95 ms. The location of this peak is the virtual electrode position. It has a pulse width of approximately 2 ms, which is twice the pulse width of the stimulating electrodes, exactly what was desired. It is roughly 200 μm wide, which is

the same width as the stimulating electrodes. Further tests will be conducted in order to determine if this size remains constant or if it varies with different electrode sizes and pitches. Finally, from Fig. 5 it can be determined that the cathodic voltage at the virtual electrode is -0.42 V. This is 0.15 V and 0.24 V lower (less negative) than the left and right electrodes respectively.

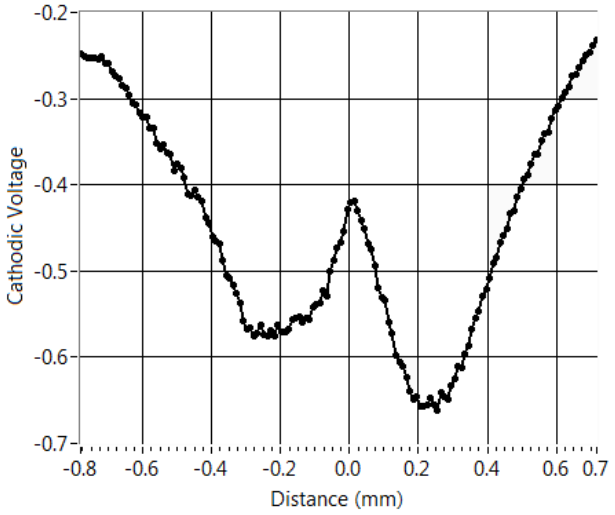

Fig. 5 Potential along cross-section of two stimulating electrodes, recorded during the cathodic spike. The two stimulating electrodes are located approximately ±0.25 mm from the center point, located at 0.0 mm. Data is recorded every 10 µm

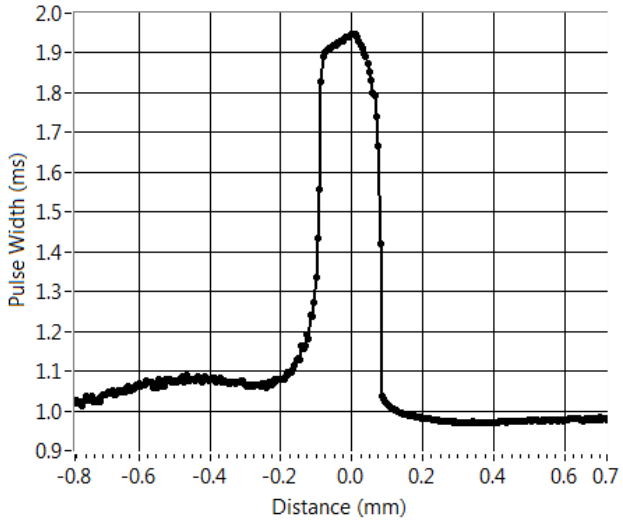

Fig. 6 Pulse width recorded along electrodes. The two stimulating electrodes are located in the exact same position as in Fig. 3, but instead of recording the potential it instead recorded the pulse width at each location. The pulse width is roughly 1 ms at the location of the two stimulating electrodes, but rises to just short of the desired 2 ms at the middle point between the two. Data is recorded every 5 µm

Reiterating the setup, in this experiment a 1 ms pulse width was used instead of 40 µs in order to obtain reliable pulse width measurements. We thus make the assumption for our proof of concept that the 1 ms pulse will act as the 40 µs and not activate a neuron, whereas a 2 ms pulse will act as the 80 µs and activate a neuron. This assumes that the behavior of the virtual electrode obtained for the longer pulses can be applied to shorter pulse widths.

In order to obtain a clearer view of how this virtual electrode would appear to a neuron, the range of pulse widths [1 ms, 2 ms] in Fig. 6 were normalized to [0, 1]. We assume pulse widths of 2 ms can activate the neurons while those of 1 ms are incapable. The normalized pulse widths are then multiplied by the cathodic voltages in Fig. 5. This makes the potential with pulse widths that could activate a neuron (multiplied by 1) remain and the potential with pulse widths that could not activate a neuron (multiplied by ~0) canceled. As a result, Fig. 7 displays only the cathodic voltages from Fig. 5 that have the correct wavelength to theoretically activate a neuron.

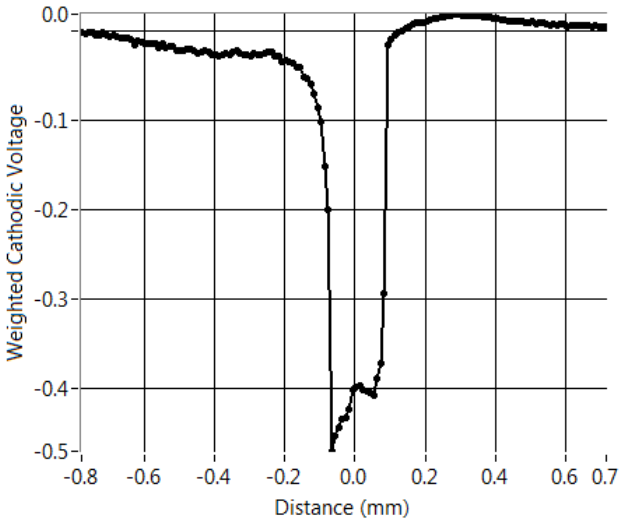

Fig. 7 Weighted voltage that could activate a neuron. This displays the cathodic voltage from Fig. 4 that is of the proper pulse width to theoretically stimulate a neuron

To further determine the virtual electrode's capability to stimulate the neuron, the activating function was taken into account. An activating function dictates whether a neuron will be activated, and this function is dependent on the second spatial derivative of the externally applied voltage resulting from a given current stimulus [14], [15]. We fist calculate and then compare the 2nd spatial derivative of the potentials recorded from a physical electrode and the virtual electrode.

In order to compare the virtual electrode to a single physical electrode, the right electrode was stimulated on its own and the potential recorded. Fig. 8 shows the cathodic voltage and its second derivative found for just the right electrode (Fig. 4 C) with a 10 µA biphasic current with a 2 ms pulse width and a 0.75 ms interphase delay. This is theoretically the same parameters as the virtual electrode. The results for the physical electrode were obtained by only stimulating the right electrode

and scanning along a cross-section of it while recording the peak cathodic voltage at each point, seen in Fig. 8 A. The resulting potential was then curve-fitted with a 100th degree polynomial in order to make the subsequent derivatives smooth. The 2nd derivative of it was then calculated (Fig. 8 B). In Fig. 8 B there is a clear peak at 0.2 mm, which is approximately where the right electrode has previously been shown to be. The peak has a value of 17 V/m^2.

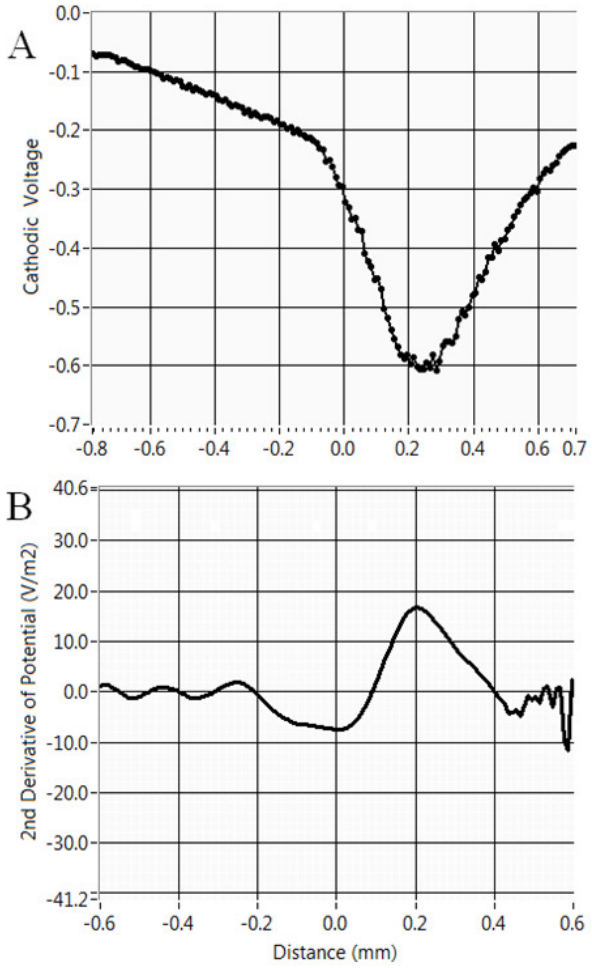

Fig. 8 [A] Cathodic voltage of right electrode stimulated with a 10 μA, 2 ms biphasic current. [B] Second spatial derivative of [A]

The same technique was then used upon the weighted voltage for the virtual electrode from Fig. 7, once again first curve-fitting the data to a 100th degree polynomial so that the derivatives are smooth, and then taking the 2nd derivative of it (Fig. 9). In Fig. 9 the peak is centered at 0.0 mm, which is where the virtual electrode was, and has a peak value of 93.7 V/m^2.

We now compare the potential and 2nd derivatives of the physical and virtual electrodes. From Figs. 7-9, even though the cathodic voltage was lower (less negative) for the virtual electrode in Fig. 7 than the physical electrode in Fig. 8 A, the second derivative of the potential is significantly larger for the virtual electrode in Fig. 9 than for the physical electrode in Fig. 8 B. This is because the virtual electrode accelerates much more steeply than the right electrode, which is what the second derivative is based upon. This is very interesting, because it suggests that the virtual electrode may be even more effective than a physical electrode at activating neurons.

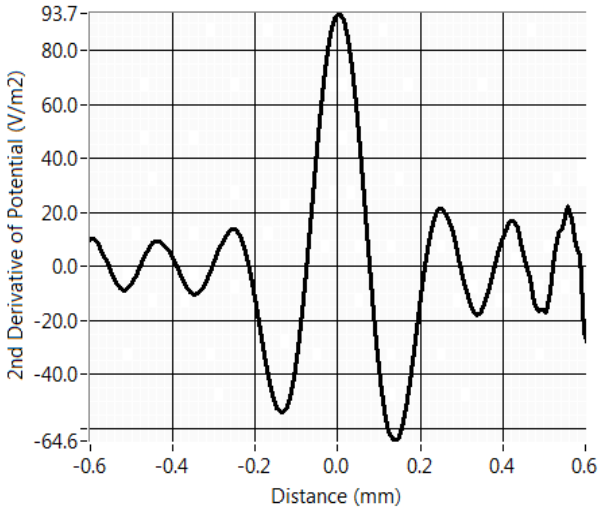

Fig. 9 Second spatial derivative of the weighted cathodic voltage from Fig. 7 The data from Fig. 7 was first curve-fitted to a 100th degree polynomial and then 2nd derivatives were taken of it

IV. Discussion and Conclusion

A. Summary of Findings

The purpose of this paper was to determine whether a virtual electrode of twice the pulse width of two stimulating electrodes could be created that would only activate neurons above the virtual electrode. We have been able to successfully demonstrate that through stimulating two adjacent electrodes with slightly time-offset signals, a waveform with twice the pulse width will appear directly between the two electrodes. Additionally, the physical width over which the virtual electrode spans seems to be comparable to the width of the stimulating electrodes, although this should be further tested with electrodes of varying sizes and spacing. In addition, we were able to weight the virtual electrode's voltage based upon pulse width and what could theoretically stimulate a neuron. From this we have shown that the potential above the virtual electrode is less than that above the stimulating electrodes. However, when the activating function is taken into account the second spatial derivative of the potential above the virtual electrode is significantly larger than that of the physical electrodes. This suggests that not only could the virtual electrode be effective in stimulating neurons, but that it may be significantly more effective than physical electrodes.

B. Suggestions for Further Research

Although these results are very promising towards the worth of a virtual electrode, there is still further research to be done. First, in this experiment, a large pulse width of 1 ms was

used instead of a 40 μs pulse width in order to obtain reliable pulse width measurements. We assume that the results obtained from longer pulses can be applied to shorter pulses, but further research should be done to determine if similar results can be found for a pulse width of 40 μs.

Second, this study used pulses of 10 μA, which is on the smaller end of useful stimulation current amplitudes. Further research should be concerned with determining whether similar results can be obtained for larger applied currents.

Third, a limitation of this study is the assumption that LabView's measurement of the pulse width accurately represents how a RGC will also respond to a given pulse width. The second derivative in Fig. 9 for the virtual electrode is based on these pulse width measurements, so if RGCs react differently, the activating function values may change as well. As such, the next step is to confirm these results by actually seeing if a virtual electrode composed of two 40 μs pulses could be used to stimulate real RGCs.

C. Conclusion

This paper presents a stimulation technique that may be used to maximize the efficacy of electrode arrays by offering the capability of additional, virtual electrodes. These virtual electrodes can be created in between any two electrodes, and are composed of two time-offset biphasic pulses that combine to form a single biphasic pulse of twice the pulse width in the center. This technique requires no new technological modification of current electrode arrays, so it can be immediately implemented into a retinal prosthetic system by simply modifying the stimulation parameters. Through this technique retinal prosthetics can further increase their resolution without the need to add additional electrodes, which ultimately will help offer fuller, clearer vision to those who suffer from retinal degenerative diseases.

ACKNOWLEDGMENT

The author would like to thank Dr. Chih-Wei Chang for his technical support and discussion.

REFERENCES

[1] Stone J L, Barlow W E, Humayun M S, Dejuan E and Milam A H. Morphometric analysis of macular photoreceptors and ganglion-cells in retinas with retinitis-pigmentosa *Arch. Ophthalmol*. Vol. 110 pp. 1634–9, 1992.

[2] Sekirnjak C, Hulse C, Jepson L H, Hottowy P, Sher A, Dabrowski W, Litke A M and Chichilnisky E J. Loss of responses to visual but not electrical stimulation in ganglion cells of rats with severe photoreceptor degeneration *J. Neurophysiol*. Vol. 102 pp. 3260–9, 2009.

[3] Humayun M S, Weiland J D, Fujii G Y, Greenberg R, Williamson R, Little J, et al. Visual perception in a blind subject with a chronic microelectronic retinal prosthesis *Vis. Res*. Vol. 43 pp. 2573–81, 2003.

[4] Yanai D, Weiland J D, Mahadevappa M, Greenberg R J, Fine I and Humayun M S. Visual performance using a retinal prosthesis in three subjects with retinitis pigmentosa *Am. J. Ophthalmol*. Vol. 143 pp. 820–7, 2007.

[5] Ahuja A K, Dorn J D, Caspi A, McMahon M J, Dagnelie G, Dacruz L, Stanga P, Humayun M S and Greenberg R J Blind subjects implanted with the Argus II retinal prosthesis are able to improve performance in a spatial-motor task *Br. J. Ophthalmol.* Vol. 95 pp. 539–43, 2011.

[6] Hecht, Eugene. *Optics*, 2nd Ed, Addison Wesley, 1987.

[7] McCreery D B, Agnew W F, Yuen T G H and Bullara L Charge density and charge per phase as cofactors in neural injury induced by electrical stimulation *IEEE T. Bio-Med. Eng*. Vol. 37 pp. 996–1001, 1990.

[8] Weiland JD, Liu W, Humayun MS Retinal Prosthesis. *Annu Rev Biomed Eng* Vol. 7 pp. 361-401, 2005.

[9] Khalili M G, Lovell N H, Wilke R G, Suaning G J, Dokos S. Performance optimization of current focusing and virtual electrode strategies in retinal implants *Comput. Meth. Prog. Biomed.* To be published.

[10] Charles T, Choi M, Hsu C H. Conditions for generating virtual channels in cochlear prosthesis systems. *Ann. of Biomed. Eng.* Vol. 37 pp. 614-24, 2009.

[11] Suzuki S, Humayun M S, Weiland J D, Chen S J, Margalit E, Piyathaisere D V, et al. Comparison of electrical stimulation thresholds in normal and retinal degenerated mouse retina, *Jpn J Ophthalmol*, Vol. 48 pp. 345–9, 2004.

[12] Lo Y, Chen K, Gad P, Liu W A fully integrated high compliance voltage soc for epi-retinal and neural prostheses *IEEE Trans. Biomed. Circuits Sys*. Vol. 7 pp. 761–72, 2013

[13] Jensen R J, Rizzo J F, Grumet A E, Edell D J, Wyatt J L Single unit recording following extracellular electrical stimulation of rabbit retinal ganglion bodies. *Technical Report 600, MIT Research Laboratory of Electronics*, 1996

[14] Rattay F, Aberham M. Modeling axon membranes for functional electrical stimulation *IEEE T. Bio-Med. Eng.* 40 pp. 1201-1209, 1993.

[15] Coburn B. Neural modeling in electrical stimulation *Critic. Rev. Biomed. Eng*. Vol. 17 pp. 133-78, 1989